Optimization and performance criteria of a Stokes polarimeter based on two variable retarders

Alba Peinado[1], Angel Lizana[1,*], Josep Vidal[1,2], Claudio Iemmi[3] and Juan Campos[1]

[1]*Department of Physics, Universitat Autònoma de Barcelona, 08193, Bellaterra, SPAIN*
[2]*ALBA Synchrotron Light Source Facility, 08290, Cerdanyola del Vallès, SPAIN*
[3]*Departament of Physics, Universidad de Buenos Aires, 1428, Buenos Aires, ARGENTINA*
*angel.lizana@uab.es

Abstract: In this paper we present the analysis, optimization and implementation of several Stokes polarimeter configurations based on a set-up including two variable retarders. The polarimeter analysis is based on the Mueller-Stokes formalism, and as a consequence, it is suitable to deal with depolarized light. Complete Stokes polarimeters are optimized by minimizing the amplification of simulated errors into the final solution. Different indicators useful to achieve this aim, as the condition number or the equally weighted variance, are compared in this paper. Moreover, some of the optimized polarimeters are experimentally implemented and it is studied the influence of small deviations from the theoretical ones on the amplification of the Stokes component error. In addition, the benefit of using incomplete polarimeters, when detecting specific ranges of states of polarization, is discussed.

©2010 Optical Society of America

OCIS codes: (120.5410) Polarimetry; (120.2130) Ellipsometry and polarimetry; (230.3720) Liquid-crystal devices;

References and links

1. M. Anastasiadou, A. De Martino, D. Clement, F. Liège, B. Laude-Boulesteix, N. Quang, J. Dreyfuss, B. Huynh, A. Nazac, L. Schwartz, and H. A. S. Cohen, "Polarimetric imaging for the diagnosis of cervical cancer," Phys. Status Solidi **5**(5), (2008).
2. K. M. Twietmeyer, R. A. Chipman, A. E. Elsner, Y. Zhao, and D. VanNasdale, "Mueller matrix retinal imager with optimized polarization conditions," Opt. Express **16**(26), 21339–21354 (2008), http://www.opticsinfobase.org/oe/abstract.cfm?uri=oe-16-26-21339.
3. J. L. November, and L. M. Wilkins, "The Liquid Crystal Polarimeter for solid-state imaging of solar vector magnetic fields," Proc. SPIE **2265**, 210–221 (1992).
4. A. Márquez, I. Moreno, C. Iemmi, A. Lizana, J. Campos, and M. J. Yzuel, "Mueller-Stokes characterization and optimization of a liquid crystal on silicon display showing depolarization," Opt. Express **16**, 1669–1685 (2008), http://www.opticsinfobase.org/ oe/ abstract.cfm?uri=oe-16-3-1669.
5. S. Firdous, and M. Ikram, "Stokes Polarimetry for the Characterization of Bio-Materials using Liquid Crystal Variable Retarders," Proc. of the SPIE-OSA Biomedical Optics **6632**, 66320F–1 66320F–13 (2007).
6. R. A. Chipman, "Polarimetry," in *Handbook of Optics*, 2nd ed., McGraw-Hill, (New York, Chapter 22, 1995).
7. D. S. Sabatke, M. R. Descour, E. L. Dereniak, W. C. Sweatt, S. A. Kemme, and G. S. Phipps, "Optimization of retardance for a complete Stokes polarimeter," Opt. Lett. **25**(11), 802–804 (2000).
8. H. J. Coufal, D. Psaltis, and B. T. Sincerbox, *Holographic Data Storage*, (Springer-Verlag, Berlin,2000).
9. R. Dou, and M. K. Giles, "Closed-loop adaptive-optics system with a liquid-crystal television as a phase retarder," Opt. Lett. **20**(14), 1583–1585 (1995).
10. J. Turunen, and F. Wyrowski, *Diffractive Optics for Industrial and Commercial Applications*, (Akademie Verlag, Berlin, 1997).
11. E. Garcia-Caurel, A. De Martino, and B. Drévillon, "Spectroscopic Mueller polarimeter based on liquid crystal devices," Thin Solid Films **455–456**, 120–123 (2004).
12. J. M. Bueno, "Polarimetry using liquid-crystal variable retarders: theory and calibration," J. Opt. A, Pure Appl. Opt. **2**(3), 216–222 (2000).
13. A. De Martino, Y. K. Kim, E. Garcia-Caurel, B. Laude, and B. Drévillon, "Optimized Mueller polarimeter with liquid crystals," Opt. Lett. **28**(8), 616–618 (2003).

14. J. Zallat, S. Aïnourz, and M. Stoll, "Optimal configurations for imaging polarimeters: impact of image noise and systematic errors," J. Opt. A, Pure Appl. Opt. **8**(9), 807–814 (2006).
15. F. Goudail, "Noise minimization and equalization for Stokes polarimeters in the presence of signal-dependent Poisson shot noise," Opt. Lett. **34**(5), 647–649 (2009).
16. D. Lara, and C. Paterson, "Stokes polarimeter optimization in the presence of shot and Gaussian noise," Opt. Express **17**(23), 21240–21249 (2009), http://www.opticsinfobase.org/abstract.cfm?URI=oe-17-23-21240.
17. V. L. Gamiz, and J. F. Belsher, "Performance limits of a four-channel polarimeter in the presence of detection noise: Non-Ideal polarimeter," Opt. Eng. **41**, 973–980 (2002).
18. P. Taylor, *Theory and Applications of Numerical Analysis*, (Academic Press, London, 1974).
19. R. C. Jones, "A new calculus for the treatment of optical systems," J. Opt. Soc. Am. A **31**(7), 488–493 (1941).
20. R. M. A. Azzam, and N. M. Bashara, *Ellipsometry and Polarized Light*, (North-Holland, Amsterdam, 1977).
21. D. Goldstein, *Polarized Light*, (Marcel Dekker, NY, 2003).
22. G. E. Forsythe, M. A. Malcolm, and C. B. Moler, *Computer Methods for mathematical computations*, (Prentice-Hall, New Jersey, 1977).
23. E. Compain, S. Poirier, and B. Drevillón, "General and self-consistent method for the calibration of polarization modulators, polarimeters, and mueller-matrix ellipsometers," Appl. Opt. **38**(16), 3490–3502 (1999).
24. J. S. Tyo, "Noise equalization in Stokes parameter images obtained by use of variable-retardance polarimeters," Opt. Lett. **25**(16), 1198–1200 (2000).
25. S. R. Davis, R. Uberna, and R. A. Herke, "Retardance sweep polarimeter and method," United State Patent, patent US 6744509 B" (2004).

1. Introduction

Polarimetric techniques are widespread used in many research fields as medical physics [1, 2], astronomy [3], polarizing sample characterization [4, 5], among others. In all these applications, the knowledge of the state of polarization of light beams or the polarizing properties of samples is essential. The basic instrument used to perform these measurements is a polarimeter device.

Polarimeters can be sub-divided in different types, for instance, as a function of the information that they provide or the specific characteristics of the polarimeter constituent elements [6]. A Stokes polarimeter is a device that allows us to determine the state of polarization (SOP) of a light beam by measuring its corresponding Stokes parameters. In particular, a Stokes polarimeter requires the use of a polarization state detector (PSD) which is typically formed by polarizing elements as waveplates and polarizers. Then, the Stokes parameters of the analyzed light beam are obtained by taking different radiometric measurements corresponding to the projection of the SOP of the light beam over the corresponding SOPs detected by different configurations of the PSD elements, i.e. different polarization analyzers. In addition, the Stokes polarimeter is said complete if it allows obtaining the four Stokes parameters that describe the analyzed light beam. On the contrary, it is said incomplete when only a part of the whole polarimetric information is available.

For a complete description of the SOP of a light beam, some Stokes polarimeters require of manual or mechanical movements of their polarizing elements. In this sense, some particular polarimeters based on passive polarizing elements are reported in the literature, as for instance in Ref [7], where a complete Stokes polarimeter based on a fixed polarizer and a rotating waveplate with a fixed retardance is presented. This type of polarimeters can be very accurate because they generate redundant information which may be used to diminish the influence of different noise sources. However, they also present some practical disadvantages because mechanical moving parts are required and a limitation in the utilizable optical bandwidth is imposed by the fixed retardance waveplates.

Due to the light beam modulation capability that liquid crystal (LC) technology offers, LC devices are widespread used in a large number of optical applications [8–10]. Recently, LC based devices have been also applied in the implementation of polarimeters [11, 12]. Some features of liquid crystals, as its birefringence and the possibility of orientating its molecules with an applied voltage, give them the capability to perform as variable waveplates whose retardance varies as the addressed voltage is changed. Thus, any mechanical moving part is required in polarimeters based on LC variable retarders, avoiding vibrations and positioning errors. Moreover, the retardance values of the LC can be properly chosen in order to optimize

its performance as a function of the specific wavelength used. As an example, in Ref [13]. the optimization of a polarimeter based in two LC variable retarders and a polarizer is described.

When developing strategies oriented to optimize the polarimeter accuracy it is important to minimize the influence of different instrumental errors on the final measurement values. In order to diminish the effect of noise in the final measurements, some studies have been carried out [7, 13–17]. For instance, different indicators as the condition number (*CN*) [18] or the equally weighted variance (*EWV*) [7] have been used in optimization procedures.

In this work we present the analysis, optimization and implementation of complete Stokes polarimeters based on a set-up including two variable retarders. For the optimization process, we have used different optimization criteria in order to analyze their suitability when increasing the number of polarization analyzers or when analyzing specific ranges of states of polarization. Moreover, a study of the effect of small deviations of the optimized polarimeter when performing the experimental implementation is also provided. Therefore, we think that this paper can be understood not only as an exhaustive analysis of the optimization and performance criteria of polarimeters based on variable retarders but also a useful guideline for these applications where it is required to design or to experimentally implement a polarimeter device.

The outline of this paper is as follows. In section 2, a mathematical description of polarimeters and a review of different indicators useful to perform polarimeter optimizations are presented. In section 3, the optimization of diverse polarimeters configurations as a function of the number of polarization analyzers is done. Moreover, an analysis of the variations of the *CN* and the *EWV* with the number of polarization analyzers is also conducted. In addition, the suitability of incomplete polarimeters under certain conditions is revised. In section 4, the experimental methodology used for the implementation of Stokes polarimeters is provided. The implemented polarimeters are tested by measuring different incident SOPs and the obtained results are compared with those provided by a commercial polarimeter.

2. Polarimeter mathematical description and optimization criteria

The mathematical description of a polarimeter can be done by using different mathematical formalisms, as for instance, those developed by Jones [19] or Berreman [20]. In this work we use the Mueller-Stokes (M-S) formalism because it takes into account depolarized light and allows determining the SOP of a light beam just by taking intensity measurements behind a PSD.

On one hand, in the M-S description, a SOP is fully determined by means of the four elements of the so-called Stokes vector. These four real parameters give information about: the total intensity S_0 of the light beam, the intensity difference between horizontal and vertical linear polarized components S_1, the intensity difference between ±45° linearly polarized components S_2 and the intensity difference between right and left circularly polarized components S_3. On the other hand, the interaction of light beams with polarizing samples is described by means of Mueller matrices, which are 4x4 real matrices that relate the incident S_{in} and the exiting S_{ex} Stokes vectors as follows:

$$\mathbf{S}_{ex} = \mathbf{MS}_{in} \tag{1}$$

where *M* is the Mueller matrix. The first component of the exiting Stokes vector corresponds to the intensity of the light beam which is transmitted, reflected or scattered by the polarizing sample. This value corresponds to the dot product of the incident state of polarization, described by the Stokes vector S_{in}, with the first row of the Mueller matrix *M*. If the matrix *M* is describing a particular configuration of a PSD, the exiting power is the projection of the incident SOP over the SOP described by the first row of *M* that corresponds to a given polarization analyzer. Therefore, if the incident SOP is equal to the selected polarization analyzer, the power detected behind the PSD is maximal.

By performing different radiometric measurements corresponding to the projection of a given incident state of polarization **S** over diverse configurations of the PSD (i.e. different polarization analyzers) a linear equation system is built. Mathematically, the linear equation system is described by the following equation:

$$\mathbf{I} = A\mathbf{S} \tag{2}$$

where **I** is a nx1 column vector containing the set of radiometric measurements and A is a nx4 matrix whose rows are the Stokes parameters of the SOP fully transmitted at the different polarization analyzers.

Given a well-known matrix A (i.e. well-calibrated polarimeter) and a vector of measures **I**, the value of **S** can be obtained just by solving Eq. (2). Note that for a fully description of the solution **S**, a minimum number of four independent polarization analyzers are required. Moreover, we can distinguish two different situations by taking into account if the number n of polarization analyzers is equal or higher than four. On one hand, when the matrix A of Eq. (2) is a non-singular square matrix (n=4), its inverse A^{-1} exists and it is unique, leading to Eq. (3). On the other hand, if more than four polarization detectors are used (n>4), A is a nx4 rectangular matrix and in general no solution exists. However, we can find a solution that minimizes the mean square error by the use of the pseudoinverse $\tilde{A}^{-1}$ which is defined in Eq. (4):

$$\mathbf{S} = A^{-1}\mathbf{I} \tag{3}$$

$$\mathbf{S} = \left(A^{\mathrm{T}}A\right)^{-1}A^{\mathrm{T}}\mathbf{I} = \tilde{A}^{-1}\mathbf{I} \tag{4}$$

where A^{-1}, A^{T} and $\tilde{A}^{-1}$ are the inverse, the transpose and the pseudoinverse of the matrix A, respectively.

Therefore, according to the matrix A, we can use Eq. (3) or Eq. (4) to obtain an experimental measurement of the incident SOP. As previously stated, by using four linearly independent polarization analyzers, the corresponding polarimeter is complete (i.e. it performs a complete polarimetric characterization of the incident SOP). In the case of complete polarimeters, the representation of the polarization analyzers upon the Poincaré sphere [21] defines a curve not included in a plane, and so, enclosing a volume.

An infinite number of matrices A formed by diverse sets of polarization analyzers are able to describe complete polarimeters. Nevertheless, in presence of noise, every matrix A transmits the error in a different way. In fact, as a consequence of the non idealistic optical elements used in the real experimental set-ups (as for instance rotation stage mis-positioning, retardance values deviation or intensity measurements errors), the values of the measured SOP always present an associated error.

Let's analyze the effect of noise within the intensity vector **I**. In this case, Eq. (3) and (4) become as follows:

$$\mathbf{S} + \mathbf{\Delta S} = A^{-1}\left(\mathbf{I} + \mathbf{\Delta I}\right) \tag{5}$$

$$\mathbf{S} + \mathbf{\Delta S} = \tilde{A}^{-1}\left(\mathbf{I} + \mathbf{\Delta I}\right) \tag{6}$$

where Δ**I** is the error associated to the intensity measurements and Δ**S** the solution transmitted error.

In order to optimize the design of polarimeters it is very important to determine the sensitivity of the linear solution to experimental errors in the measurements. With the aim of minimizing the noise transmitted through the matrix inversion from the vector **I** to the solution **S**, in this work we compare three different indicators: the condition number (*CN*) [18], the Equally Weighted Variance (*EWV*) [7] and the error associated at every component

of the Stokes vector [14]. Whereas the *CN* quantifies if the matrix A^{-1} is well-conditioned (i.e. far to be singular), the *EWV* and the variance associated at every component of *S* are related with the propagation of errors from the vector *I* to the solution *S*.

The theoretical minimum value of *CN* is equal to 1, which is obtained for unitary matrices as they do not amplify the error. Note that in our case every row of a given matrix *A* is formed by four elements that describe a polarization analyzer, being the first parameter the intensity of the specific SOP analyzed. Then, all the coefficients of the first column are equal to one when normalized and *A* is never a unitary matrix. As a consequence, the value 1 for *CN* can never be obtained. However, by minimizing the *CN* of a set of possible *A* matrices, we obtain the best conditioned matrix, and so, the closest to a unitary matrix. When *A* is not a square matrix the singular value decomposition theorem [22] can be used, leading to a product of two orthonormal matrices with a diagonal matrix. In these cases, the definition of the *CN* is not unique. Particularly in this work we have used the definition given in the next equation:

$$CN(A) = \frac{\sigma_{max}}{\sigma_{min}} \tag{7}$$

where σ_{max} and σ_{min} are the maximum and minimum singular values different from zero of the matrix *A*.

We want to emphasize that although *CN* is a very good indicator to measure the condition of a matrix, it does not take into account data redundancy. To take into account the improvement given by data redundancy, we can use the *EWV* criterion [7], which indicates the transmission of the variance from *I* to *S*:

$$EWV(A) = \sum_{j=0}^{R-1} \frac{1}{\sigma_j^2} \tag{8}$$

where *R* is the rank of the matrix *A* and all its singular values σ_j are contributing in the summation of Eq. (8). The *EWV* indicator provides a useful estimation of the global error amplification in the solution vector *S* when some amount of noise is present in the intensity measurements vector *I*. This global error is the summation of the specific errors transmitted to every component of the Stokes vector. As a consequence, the minimized global transmitted error, obtained by optimizing the *EWV* indicator, not always gives place to the minimum error of every Stokes parameter. In order to study the sensitivity of the Stokes parameters error in presence of noise, we can analyze the error propagation corresponding to the linear equation system described in Eq. (4). Let us rewrite Eq. (4) as follows:

$$\mathbf{S} = \tilde{A}^{-1}\mathbf{I} = Q\mathbf{I} \Rightarrow S_i = \sum_{k=1}^{N} q_{ik} I_k \tag{9}$$

with $i = (0,1,2,3)$ and where N is the number of elements of the intensity vector *I*. Moreover, q_{ik} represent the coefficients of the pseudoinverse matrix $\tilde{A}^{-1}$ and S_i are the components of the Stokes vector *S*. By applying error propagation in Eq. (9), and considering only errors in the vector *I* coefficients (ideal q_{ik} coefficients), we obtain the next equation:

$$\delta S_i = \left[\sum_{k=1}^{N} \left(\frac{\partial S_i}{\partial I_k} \right)^2 \delta I_k^2 \right]^{\frac{1}{2}} = \delta I \left[\sum_{k=1}^{N} \left(\frac{\partial S_i}{\partial I_k} \right)^2 \right]^{\frac{1}{2}} \tag{10}$$

It has been assumed that the statistical noise is uniformly distributed on the components of vector *I* ($\delta I_k = \delta I$). Then, Eq. (9) and (10) lead to the following expression of the error associated at every component of the Stokes vector:

$$\delta S_i^2 = \delta I^2 \sum_{k=1}^{N} q_{ik}^2 \qquad (11)$$

note that the summation of the four δS_i of the obtained Stokes vector is equivalent to the *EWV*.

Equation (11) shows the error amplification corresponding to every parameter of the solution vector S in presence of noise in the intensity measurements vector I. However, in a more realistic situation, we have to take also into account the contribution of errors in the coefficients q_{ik} of the matrix Q (see Eq. (9)) to the final Stokes parameters errors. In addition, the errors in the matrix coefficients depend on the specific matrix calibration process used, as for instance the one given in [23].

3. Polarimeter optimization process

In this section, a polarimeter optimization process, based on the minimization of some well-known mathematical indicators (see section 2), is presented. This method is applied to the optimization of a complete and non-mechanical polarimeter based on two variable LC waveplates. The set-up of the polarimeter to be optimized is sketched in Fig. 1. The device is formed by a linear polarizer (PL) at 0° to the laboratory vertical and two LC waveplates oriented at 45° (WP$_1$) and at 0° (WP$_2$). The LC waveplates retardance values (φ_1 and φ_2, respectively) can be electronically varied.

The described system could be used both, as a Polarization State Generator (PSG) if it is illuminated with a monochromatic light source (according to Fig. 1(a)), or as a Polarization State Detector (PSD) if a monochromatic light beam impinges on it and the intensity is detected by a radiometer (according to Fig. 1(b)). It is clear that for a given retardances configuration (φ_1, φ_2) of the waveplates a specific SOP will be generated by the PSG, then if a beam with the same SOP would be used to illuminate the system when acting as PSD the intensity detected would be maximal. In addition, any other possible SOP projected over this polarization analyzer gives lower intensity values.
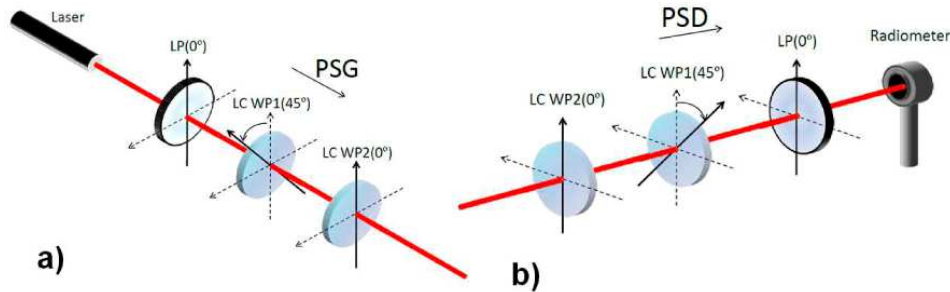

Fig. 1. Set-up of the LC based polarimeter: a) PSG; b) PSD.

The set of polarization analyzers that is available by using the polarimeter shown in Fig. 1 can be obtained just by determining the set of SOPs that can be generated with it. In fact, the set of polarization analyzers available is analogous to the set of SOPs that can be generated. The SOPs available when using the PSG are calculated by taking into account Eq. (1) and by multiplying the SOP exiting of a linear polarizer at 0° with the Mueller matrices of the corresponding WP$_1$ and WP$_2$ waveplates [21]:

$$\mathbf{S}_{polarimeter} = \left(S_0, S_1, S_2, S_3\right)^T = \left(1, \cos\varphi_1, \sin\varphi_2 \sin\varphi_1, \cos\varphi_2 \sin\varphi_1\right)^T \qquad \textbf{(12)}$$

The Stokes vector given in Eq. (12) is normalized and so, its first parameter S_0 is equal to the unity. Note that the parameters S_1, S_2 and S_3 of the Stokes vector are equivalent to spherical coordinates. It is useful to represent the SOPs given in Eq. (12) over the Poincaré sphere [21]. In the Poincaré sphere representation, the lineal SOPs are mapped on its equator.

Circular SOPs are represented in the sphere poles. Finally, any other place upon the Poincaré sphere is mapping a specific elliptical SOP. By taking into account Eq. (12) we note that every locus over the Poincaré sphere is given by a pair of retardances (φ_1, φ_2). Thus, by using the set-up sketched in Fig. 1, any fully polarized SOP can be generated and any fully polarized polarization analyzer can be used. By choosing four pairs of retardances, leading to four independent SOPs analyzers, the resultant polarimeter is complete. As the LC based polarimeter allows the detection of any polarization analyzer, it is suitable to perform a study of a Stokes polarimeter optimization, for instance, by minimizing the *CN*.

Then, in order to minimizing the *CN* of square matrices *A* (whose rows are the different polarization analyzers) a data computing process is applied. It begins with *n* polarization analyzers randomly chosen, then, a MATLAB optimization function minimizes the *CN* for different sets of *n* polarization analyzers, starting from the first random set. After that, the process is repeated *N* times and in every step, a new set of starting random polarization analyzers is used. The global *CN* with the minimum value and its corresponding *A* matrix are the solution of the optimization process.

By applying this optimization for *n*=4, the process leads to four polarization analyzers that represented upon the Poincaré sphere correspond to the vertexes of a regular tetrahedron. This result is in agreement with previous studies, as an example in [7]. By repeating the optimization process, in all the cases we have obtained regular tetrahedrons with the same *CN* and with different orientations. Therefore, any of the infinite regular tetrahedrons inscribed into the Poincaré sphere gives the best solution when optimizing polarimeters with four polarization analyzers. An example of an obtained regular tetrahedron is plotted at Fig. 2(a), where the surface of the Poincaré sphere has been erased for a higher clarity.

The optimization process can also be applied to rectangular matrices *A* corresponding to *n*>4 polarization analyzers. In particular, we have performed the process for values of *n* that correspond to the number of the vertexes of the so-called Platonic Solids (*n*=4, 6, 8, 12 and 20). By using *n*=6, *n*=8, *n*=12 and *n*=20 polarization analyzers in the optimization process, the obtained analyzers are placed respectively into the vertexes of an octahedron, of a cube, of an icosahedron and of a dodecahedron, if represented upon the Poincaré sphere (Fig. 2(b)-2(e)). These results show that the number *n* of polarization analyzers used for the design of the polarimeter corresponds to the vertexes of regular polyhedrons, if exists for the specific number *n*. Regular polyhedrons have vertexes at the same distance (same length of the edges) which maximize the Poincaré sphere enclosed volume. By maximizing the volume, the corresponding matrix *A* is moving away from singular matrices and so, approaching to unitary matrices (i.e. leading to the minimum possible *CN*). In other words, the regular polyhedrons result in polarimeters whose noise propagation of the intensity measurements is minimized.
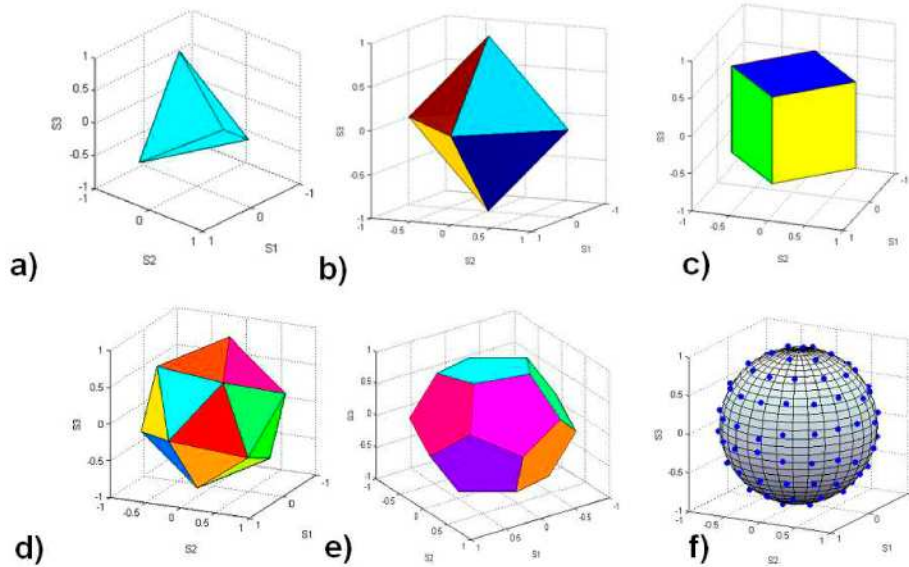
Fig. 2. *CN* minimization for: (a) four, (b) six, (c) eight, (d) twelve, (e) twenty and (f) one hundred polarization analyzers. The vertexes of the regular polyhedrons are located upon the surface of the Poincaré sphere.

Finally, we have applied the optimization process to a large number (*n*=100) of polarization analyzers. Note that this value has no equivalence into the Platonic Solids group. Nevertheless, as expected, when the obtained analyzers are represented upon the surface of the Poincaré sphere (Fig. 2(f)) they exhibit an equidistant distribution in order to maximize the enclosed volume.

To analyze the sensibility of the *CN* with data redundancy, we have studied how this parameter varies as a function of the number of polarization analyzers *n* used. The results are plotted in Fig. 3(a) where the optimized *CN* evolution as a function of the number *n* is plotted. In particular, we have calculated the *CN* corresponding to nine different optimized polarimeter configurations obtained when using *n*=4, *n*=6, *n*=8, *n*=12, *n*=20, *n*=40, *n*=60, *n*=80 and *n*=100 analyzers. We observe that the conditional number is not affected by increasing the number of analyzers, showing an almost constant value. In fact, the value obtained for the different optimized polarimeter configurations is very similar to the one obtained in Ref [24]. ($CN = \sqrt{3}$), where a polarimeter with four polarization analyzers is optimized. The *CN* value is not affected by increasing the number of data because the redundancy data equally affects the maximum σ_{max} and minimum σ_{min} singular values of the matrix *A* and so, this information is lost in the division of Eq. (7).

As it is well-known, data redundancy in experiments leads to better results as a consequence of the experimental error minimization. In order to detect this improvement in the optimized configurations, we have used the *EWV* criteria. In fact, we have analyzed the behavior of the *EWV* indicator when increasing the number of polarization analyzers. Then, for every set of *n* polarization analyzers, corresponding to a *CN* minimization obtained by using the MATLAB optimization function, the *EWV* indicator is also calculated. The obtained results, shown in Fig. 3(b), indicate that the *EWV* values decreases, by following an asymptotic behavior, as the *A* matrix dimensions increases.
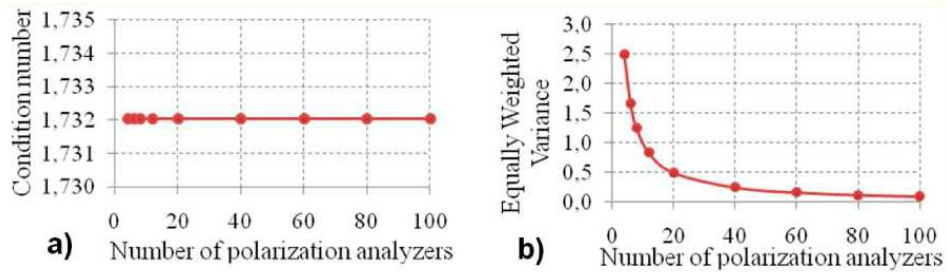
Fig. 3. Analysis of: (a) *CN*; (b) *EWV* as a function of the polarization analyzers number.

In applications where the detection of only a specific range of SOPs is required, it is interesting to study how the presence of noise in the measurements affects each Stokes parameter. Therefore, by following Eq. (11), where we have assumed $\delta I=1$, we have calculated the variance of the Stokes components for polarimeters represented by different matrices *A*. Moreover, we have also calculated the summation of the obtained variance values (ST), which is equal to the *EWV* indicator.

The study has been done for the set of four polarization analyzers shown in Fig. 2(a) (corresponding to the regular tetrahedron), the set of eight analyzers shown in Fig. 2(c) (cube) and for the set of twenty analyzers shown in Fig. 2(e) (regular dodecahedron). The simulations have been repeated for different angles of rotation θ of the different regular polyhedrons (optimized polarimeters) with respect to the three axis of the Poincaré sphere. In Fig. 4, where ordinate axes are not in the same scale in order to provide a higher visualization, we have plotted the results obtained for a complete rotation of the optimized tetrahedron (Fig. 4(a)), the optimized cube (Fig. 4(b)) and the optimized dodecahedron (Fig. 4(c)) with respect to the S_3 axis. However, we want to emphasize that the same results has been obtained for any other regular polyhedron tested or any other rotation axis chosen.
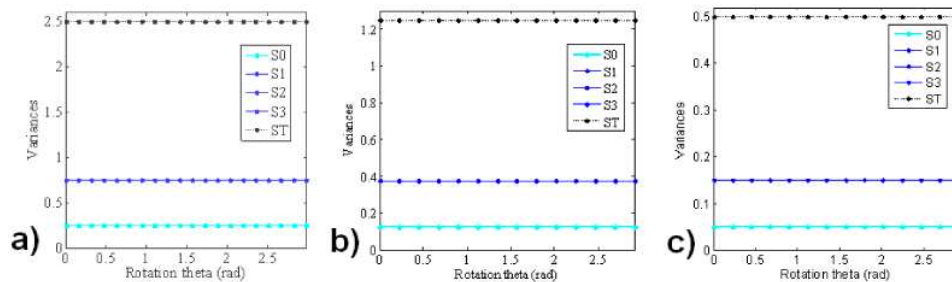

Fig. 4. Variances of S_0, S_1, S_2, S_3 and ST (Eq. (11) for different values of the rotation angle:a) Regular tetrahedron, b) Cube, c) Regular dodecahedron.

Figure 4 shows that for a specific optimized polarimeter, all performed rotations lead to the same variance of the Stokes components (and thus, the same *EWV* (ST)). This is due to the equidistant distribution of polarization analyzers, typical of optimized polarimeters. Thus regular polyhedrons do not provide a privileged SOPs range detection.

For the optimized tetrahedron (Fig. 4(a)), the parameters S_1, S_2 and S_3 show exactly the same variance value (0.75), being smaller the value for S_0 (0.25). For the case of the cube (Fig. 4(b)), whereas the variances of the parameters S_1, S_2 and S_3 are equal to 0.375, the variance of the parameter S_0 is equal to 0.125. Finally, the regular dodecahedron (Fig. 4(c)) shows the smaller variances, being the variance in the parameters S_1, S_2 and S_3 equal to 0.15 and the variance in the parameter S_0 equal to 0.05. We see as increasing the number of polarization analyzers *n*, the variances of the Stokes parameters show a remarkable reduction

that is not taken into account by using the *CN* criteria. Finally, we want to emphasize that in every case, the addition of the obtained variance values, as expected, gives the *EWV* indicator.

Next, we have analyzed the variance evolution of the Stokes parameters when rotating non-optimized sets of polarization analyzers. In fact, we have studied three different cases: four polarization analyzers describing a tetrahedron with one of its faces representing an equilateral triangle on the Poincaré sphere equator (Fig. 5(a)), four polarization analyzers embedded into a plane (Fig. 5 (b)) and four polarization analyzers describing upon the Poincaré sphere the vertexes of an irregular tetrahedron (non equilateral faces) with a given orientation (Fig. 5(c)). The obtained results are given in Fig. 6, where the variances of the Stokes parameters of the configurations shown in Fig. 5(a)-(c) are respectively plotted in Fig. 6(a)-(c).
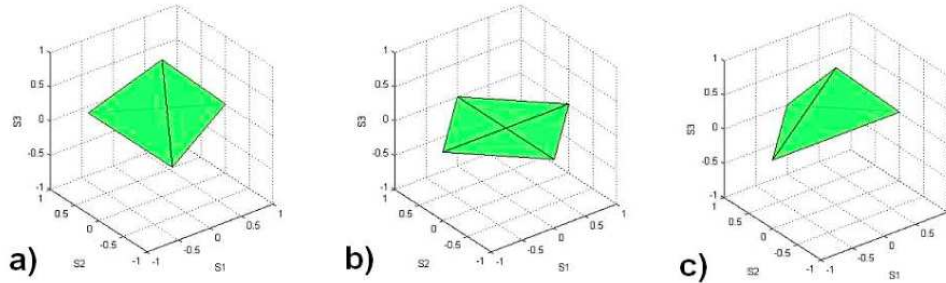

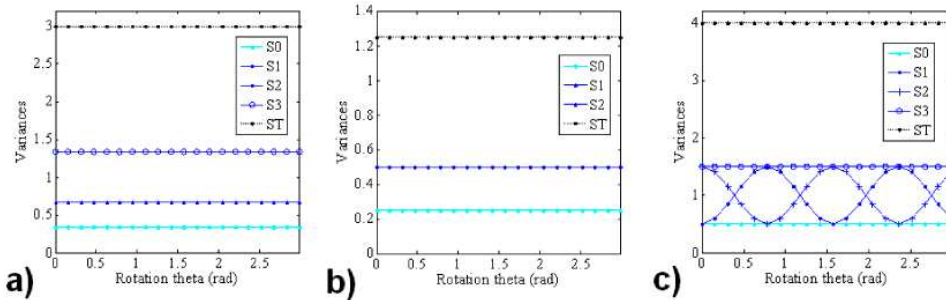Fig. 5. Different sets of four polarization analyzers.

Fig. 6. Variances of the Stokes components (Eq. (11) for the three different non-regular tetrahedrons shown in Fig. 5.

Figure 6(a) shows as the four polarization analyzers plotted in Fig. 5(a) lead to continuous values of the variance of the Stokes parameters as a function of a complete rotation around the S_3 axis. In this case, although the values corresponding to *EWV* (3.0) and the variance of S_3 (1.333) are higher than the provided by the optimized regular tetrahedron shown in Fig. 2(a), the values of the variances of S_1 and S_2 (0.667) are lower. This fact proves that a minimization of the *EWV* indicator not necessarily leads to the error minimization in each one of the Stokes parameters. In this sense, the regular tetrahedron is the best conditioned solution for *n*=4 polarization analyzers, but the irregular tetrahedron of Fig. 5(a) gives lower error amplification for linear polarized light detection due to its three equidistant polarizations analyzers placed on the Poincaré equator. For a higher insight in this issue, we have analyzed a more obvious case. In Fig. 5(b), the four polarization analyzers used are equidistantly placed at the Poincaré sphere equator and consequently, the linear polarization light detection is improved. In particular, the variances of S_1 and S_2 corresponding to this polarimeter are equal to 0.50 (Fig. 6(b)). However, as any polarization analyzer constituting this configuration provides information about the ellipiticity, the polarimeter is incomplete. Note that in this case the corresponding *CN* is equal to infinite. Finally, Fig. 6(c) shows the results

obtained when rotating around the S_3 axis the irregular tetrahedron represented in Fig. 5(c). Here, the vertexes upon the Poincaré sphere (polarization analyzers) are not equidistant and as consequence the S_1 and S_2 variances values present an oscillation as a function of the rotation angle from 0.5 to 1.5 (Fig. 6(c)). Moreover, its corresponding maxima and minima are inverted because of the non equilateral distribution of its polarization analyzers. Note that the variance of S_3 remains constant because the rotation has been performed around the S_3 axis. In addition, the obtained *EWV* is also constant and, as expected, its value is higher than the obtained with the optimized regular tetrahedron (Fig. 2(a)). However, for some orientations the variances of S_1 or S_2 show lower values. Then, the results plotted in Fig. 6(c) indicate that specific angular rotations of irregular tetrahedrons may benefit the detection of some particular state of polarization.

Summarizing, both the *CN* and *EWV* indicators are very useful for optimizing polarimeter configurations. However, in order to take into account redundancy data the use of the *CN* is not suitable. In addition, in some particular cases (as for the detection of specific SOPs ranges or for incomplete polarimeters), a selective variance minimization of the Stokes parameters, carried on by using Eq. (11), can be helpful.

Up to now we have studied different parameters in order to optimize a polarimeter but it is interesting to analyze how these magnitudes are affected when a given polarimeter is experimentally implemented.

Because of experimental errors, a real polarimeter is not exactly the desired theoretical one. However, small variations of the polarization analyzers from the ideal polarimeter give an experimental polarimeter, still well-conditioned, that minimizes the noise amplification (i.e. the values of the *CN* and the *EWV* do not differ significantly from those associated to the ideal polarimeter). In order to prove this last statement, we have simulated deviations of the polarization analyzer values (corresponding to theoretical polarimeters) and we have calculated the associated variance of the Stokes components. One hundred realizations were performed, obtaining one hundred different polarimeters deviated from the theoretical one. The variations were implemented by generating zero mean uniformly distributed random values for the polarimeter deviations with three different amplitudes: equal to 0.1, 0.3, and 0.5.

In particular, the simulations have been performed for deviations from the theoretical polarimeter shown in Fig. 2(a) (regular tetrahedron). In Fig. 7 (a)-(c), the variances of the Stokes components are represented for the different generated polarimeters as described above. It is noticeable that fluctuations of the variance of the Stokes components increase as the amplitude of the simulated deviations does. However, even for the highest amplitude used (Fig. 7(c)), the variance values are small enough to ensure an optimum performance of the associated polarimeter. The same study is applied to the set of analyzers corresponding to the dodecahedron configuration and the results are shown in Fig. 8(a)-(c). Again, by increasing the amplitude of the simulated deviations, the fluctuations on the variances of the Stokes components increase but now, as a consequence of the increment of polarization analyzers the fluctuations are remarkably lower than in the previous case. Then, although in both cases small deviations of the theoretical values give well-conditioned polarimeters, by adding redundancy an improvement in the polarimeter performance is obtained.
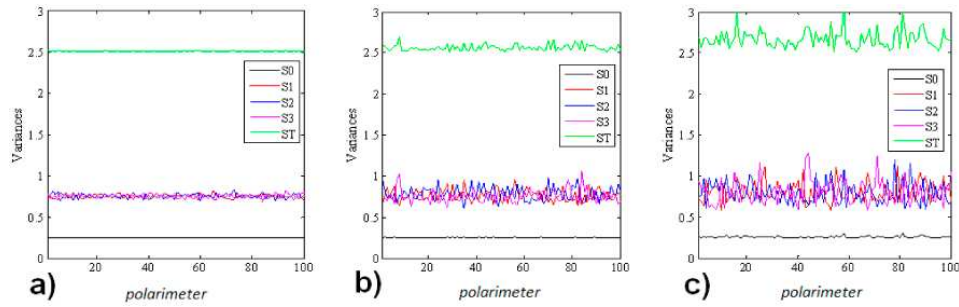
Fig. 7. Numerical simulations of the variances of S_0, S_1, S_2, S_3 and ST (Eq. (11) for 100 different polarimeters obtained from the optimized theoretical one represented in Fig. 2(a). The deviations are obtained by adding to the polarization analyzers a zero mean, uniformly distributed random numbers with amplitudes (a) 0.1; (b) 0.3; (c) 0.5.
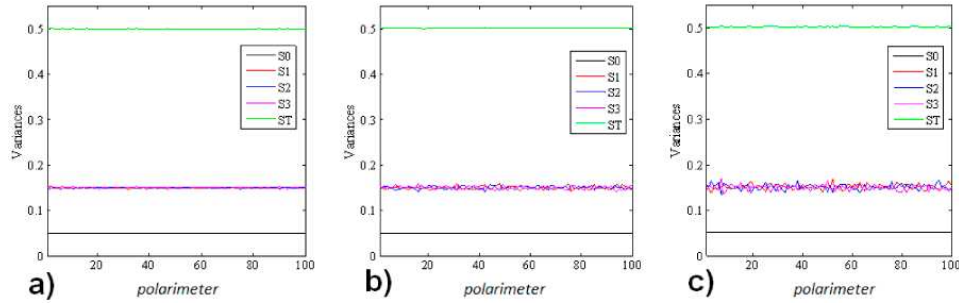

Fig. 8. Simulations of the S_0, S_1, S_2, S_3 and ST variances (Eq. (11) for 100 different polarimeters obtained from the optimized theoretical one represented in Fig. 2(e) and by adding to the polarization analyzers a zero mean; uniform distributed random numbers of amplitudes (a) 0.1; (b) 0.3; (c) 0.5.

Finally, we have repeated the same analysis but now performing deviations from the non-optimized polarimeter shown in Fig. 5(a). The Fig. 9(a)-(c) shows as whereas the deviations of the Stokes variances in S_0, S_1 and S_2 components are small, the variance in the S_3 component becomes higher. It can be understood by taking into account the non-equidistant distribution of its four polarization analyzers, resulting in a complete polarimeter but with less accuracy in the detection of elliptical SOPs. Moreover, we can see that when using non-optimized polarimeters an increasing in the deviation amplitude from the theoretical analyzers, results in polarimeters presenting higher Stokes variances values than the exhibited by optimized polarimeters with the same number of polarization analyzers (Fig. 7 (a)-(c)).
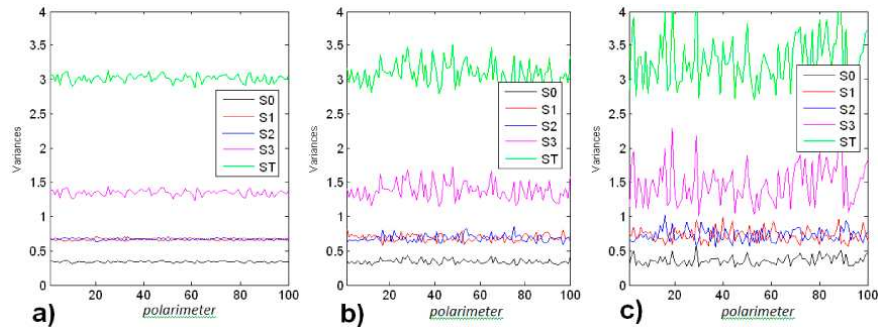

Fig. 9. Simulations of the S_0, S_1, S_2, S_3 and ST variances (Eq. (11) for 100 different polarimeters obtained from the non-optimized polarimeter represented in Fig. 5(a) and by adding to the polarization analyzers a zero mean; uniform distributed random numbers of amplitudes (a) 0.1; (b) 0.3; (c) 0.5.

4. Experimental implementation of a Stokes Polarimeter based on two variable retarders

An experimental procedure for the implementation of polarimeters based on variable retarders is described in this section. In particular, the polarimeter configurations implemented in this section are based on the set-up sketched in Fig. 1(b), where two monopixel Parallel Aligned (PA) LCDs distributed by Meadowlarks, whose retardance depends on the addressed voltage, are used as variable retarders.

Among the different possible configurations that lead to a complete polarimeter, we have chosen for implementation those corresponding to $n=4$, $n=20$ and $n=100$ analyzers represented upon the Poincaré sphere in Fig. 2(a), (e) and (f) respectively. Thus, it is required to address to each PA LCD the voltage appropriate in order to obtain the phases retardances (φ_1, φ_2) corresponding to the polarization analyzers. To this end it is necessary to calibrate the waveplates by means of a look-up table (LUT) relating the retardance with the addressed voltage. This task is carried on by using the set-up given in Fig. 10.
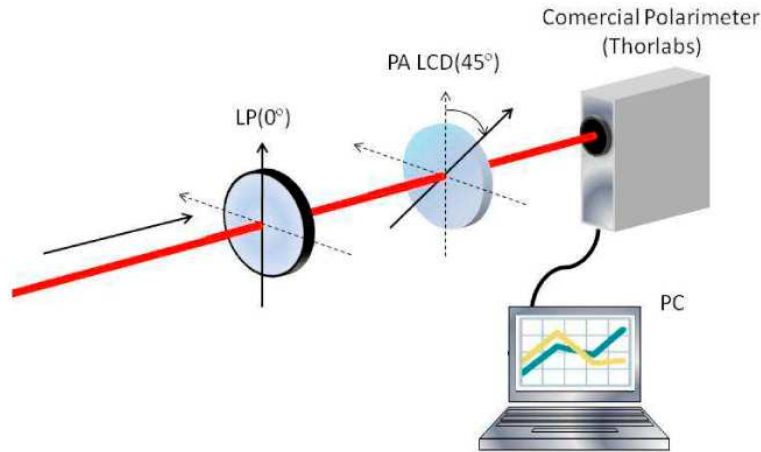

Fig. 10. Experimental set-up for the calibration of the retardance-voltatge look-up table.

The procedure to calibrate each waveplate is as follows. The PA LCD is placed at 45° of the laboratory vertical and sandwiched in between a linear polarizer LP1 (at 0°) and a commercial polarimeter (Polarization Analyzer System, PAN 5710VIS, S/N: M60217605) distributed by Thorlabs. The commercial polarimeter is based on rotating waveplates. Finally, the polarimeteric data measured with the commercial polarimeter is sent to a personal computer.

It can be proved that in the M-S formalism, the SOP of the light beam exiting from the LP1 + (PA) LCD optical system is described by the following Stokes vector:

$$\mathbf{S}_{LP1+LCD} = \left(S_0, S_1, S_2, S_3\right)^T = \left(1, \cos^2 2\theta + \cos\varphi \sin^2 2\theta, (1-\cos\varphi)\sin 2\theta \cos 2\theta, \sin\varphi \sin 2\theta\right)^T \quad (13)$$

where θ is the orientation of the LCD and φ its retardance.

Then, the SOPs (exiting from the LP1+ (PA) LCD optical system) corresponding to different addressed voltages can be experimentally obtained by using the commercial polarimeter. In particular, we have measured a set of 20 exiting SOPs for 20 different voltages uniformly distributed from 0.5V to 6V that sweep the entire range of retardations provided by the LCDs. Thus, if the exiting SOPs, corresponding to the sampled voltages are known, by fixing a rotation angle θ (45° in this case), an expression for the retardance φ can be retrieved from Eq. (13):

$$\varphi = \arctan\left(\frac{S_3 \sin 2\theta}{S_1 - \cos^2 2\theta}\right) \qquad (14)$$

where S_1 and S_3 are the Stokes parameters of the SOPs exiting from the LP1+ (PA) LCD system and θ is the orientation of the LCD equivalent retarder fast axis. Once the phase-voltage values are obtained by means of Eq. (14), a sixth-degree polynomial is used to interpolate the samples and the calibrated look-up table (LUT) is obtained and used to calculate the voltages that are necessary to achieve the optimized polarimeters shown in Fig. 2(a), (e) and (f).

The polarization analyzers optimization and the waveplates phase calibration lead to potentially well-conditioned polarimeters nevertheless, because of experimental inaccuracies, the actual polarimeter could be slightly different from the theoretical one. Then, the matrix to be used for the detection has to be calibrated. To this end we have employed a method similar to the one proposed in [25]. Four light beams with known polarization are used: Linear polarized light at 0, 90 and 45 degrees and right circularly polarized beam. The four intensities measured for each state of the actual polarimeter are denoted as I^0_i, I^{90}_i, I^{45}_i, I^{CR}_i, with $i = 0,…,$n. Then each of the four rows of our measuring matrix A (Eq. (2) is given by

$$A_{i0} = \frac{1}{2}\left(I_i^0 + I_i^{90}\right); \quad A_{i1} = \frac{1}{2}\left(I_i^0 - I_i^{90}\right); \quad A_{i2} = I_i^{45} - A_{i0}; \quad A_{i3} = I_i^{CR} - A_{i0} \qquad (15)$$
$$i = 0,...,n$$

By using the well-conditioned and experimentally calibrated matrix A we can retrieve the Stokes parameters of an incident SOP by means of Eq. (3) or Eq. (4).

Finally, we have tested three implemented complete polarimeter configurations: the tetrahedron configuration (Fig. 2(a)), the dodecahedron configuration (Fig. 2(e)) and the optimized polarimeter for one hundred polarization analyzers (Fig. 2(f)). The experimental polarimeters are tested by measuring three different incident SOPs: a linear polarized (LP) light beam at 70° of the lab vertical, a right-handed circular polarized light (CP) and an elliptical polarized light beam (EP). The measurements are compared with the results provided by the commercial polarimeter distributed by Thorlabs. The obtained results (in terms of azimuth α and ellipticity ε) are shown in Table 1. Note that the specific range of values of the azimuth angle is from 90 to −90 degrees and the corresponding to the ellipticity is from 45 to −45 degrees. In addition, all the azimuth and ellipticity angles shown in Table 1 are the average of 100 measurements of the same incident SOP. Thus, the standard deviation σ corresponding to a population of 100 samples is also provided.

In Table 1, the azimuth values α corresponding to circular light detection are not taken into account because there is not privileged orientation of the polarization ellipse in a circular polarized light. We see a good agreement between the results provided by the optimized and implemented polarimeter configurations and the measurements given by the commercial polarimeter. This agreement between data is not dependent of the specific SOP measured, pointing out the suitability of the optimization performed. Note that the standard deviation values associated to the measurements performed by using the commercial polarimeter are smaller than the obtained by using the three optimized polarimeter configurations of Table 1. It is due to the large redundancy data generated by the mechanical commercial polarimeter. However, as it is clear in Table 1, a LC-based polarimeter can also decrease the standard variance values associated to its SOPs measurements (and so, increase the repeatability of the system) by adding polarization analyzers. For instance, the standard deviations obtained by using the $n = 100$ optimized polarimeter are of the same order than the ones given by the commercial polarimeter. Finally, we want to emphasize that the experimental results given in Table 1 are an important indicator of the validity of the optimization methodology provided in this work.

Table 1. Azimuth α and Ellipticity ε values corresponding to three different measured SOPs

	Optimized Tetrahedron		Optimized Dodecahedron		n=100 Optimized Polarimeter		Commercial Polarimeter	
	α±σ(α)	ε±σ(ε)	α±σ(α)	ε±σ(ε)	α±σ(α)	ε±σ(ε)	α±σ(α)	ε±σ(ε)
LP	70.34±0.29	0.31±0.28	69.56±0.13	0.06±0.14	70.08±0.05	0.18±0.06	69.99±0.02	0.05±0.02
CP	-	44.63±0.18	-	44.31±0.11	-	44.89±0.05	-	44.72±0.02
EP	44.95±0.42	24.24±0.29	45.59±0.16	23.49±0.11	45.94±0.10	23.63±0.09	44.43±0.04	23.58±0.02

In order to test the usefulness of incomplete polarimeters when measuring specific ranges of SOPs, we have experimentally implemented the incomplete polarimeter shown in Fig. 5(b). As it is has been shown in section 3, the performed simulations indicate that this incomplete polarimeter gives lower error propagation in the components S_1 and S_2 of the Stokes vector than the complete polarimeter of Fig. 2(a). Therefore, the incomplete polarimeter is an appropriate candidate to perform linear polarized light detection. Thus, we have tested the incomplete polarimeter by measuring the linear incident SOP used in the previous study (linear polarized light at 70° of the lab (LP)). Again, the obtained value corresponds to the average of 100 measurements of the same incident SOP. In this case, the obtained result and its associated standard deviation σ is equal to 69.46±0.25.

The SOP measurement indicate a good performance of the incomplete polarimeter, obtaining lower standard deviation than the complete polarimeter optimized for the same number of polarization analyzers (the tetrahedron configuration in Table 1). Then, the incomplete polarimeter shows higher capability of measurements repeatability than the tetrahedron configuration. Therefore, an optimization of an incomplete polarimeter by minimizing the error propagation of a particular Stokes parameter is recommended for a decreasing of the noise sensibility in the detection of specific ranges of SOPs.

Throughout this work, for every pair of phases (φ_1, φ_2) used (corresponding to a given configuration of the polarimeter) a number m of intensity measurements has been taken with the radiometer. In every case, the intensity mean value has been used. In order to minimize the polarimeter detection time, we have studied the influence of the number m of intensity measurements (sample size) taken with the radiometer (see Fig. 1) on the standard deviation values σ associated to the measurements. We have performed the detection of a linear polarized light at 70° respect to the laboratory vertical with the optimized regular tetrahedron configuration (Fig. 2(a)) and with the incomplete polarimeter (Fig. 5(b)). The detection has been repeated for eight different values of radiometer sample size: 1, 10, 50, 100, 500, 1.000, 5.000 and 10.000 measurements. In all the cases, the SOP is obtained in terms of azimuth α and the SOP measurement is repeated 100 times, being calculated its corresponding standard deviation σ. The relation between the values of σ and the sample size chosen are plotted in Fig. 11, when using the complete optimized and the incomplete polarimeters.

The results show that in the sample size range from 1 to 100 samples, the standard deviation values clearly decrease. Then, by increasing the sample size range, the SOP measure repeatability of the system is improved. However, once the sample size is equal to 100, by increasing the number of intensity measurements the standard values remain almost constant. Therefore, sample sizes higher than 100 imply a magnification of the detection time without measurement repeatability benefits. In addition, in every case the standard deviation σ values corresponding to the incomplete polarimeter are lower than the obtained with the complete polarimeter, pointing out the repeatability capability of the incomplete polarimeter.
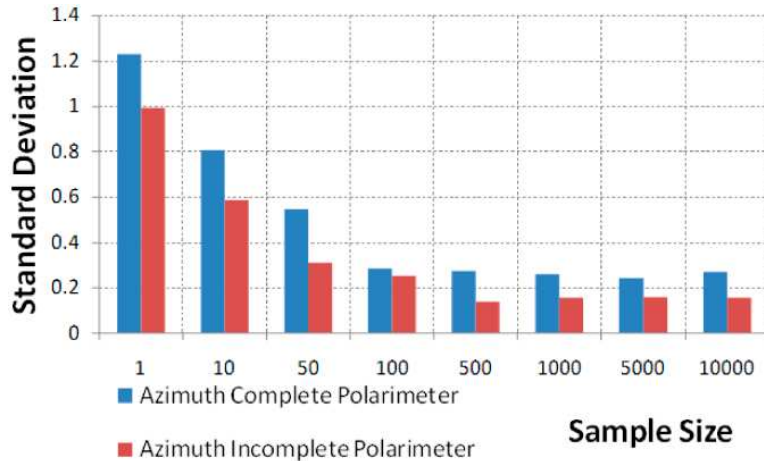
Fig. 11. Azimuth α standard deviation as a function of the number of intensity measurements (sample size) taken with the radiometer by using the optimized and the incomplete polarimeters.

5. Conclusion

In this work we have presented an analysis and comparison of diverse indicators useful for the optimization of polarimeters. In particular, for complete polarimeters, we have studied the behaviour of the *CN* and the *EWV* optimization parameters as a function of the number of polarization analyzers. We have observed that when the number of used polarization analyzers equals the number of vertexes of one of the so-called Platonic Solids, the distribution of polarization analyzers that optimize the polarimeter (minimum *CN* value) corresponds to the vertexes of the Platonic Solid when represented upon the sphere. However, we have shown as *CN* is independent of the number of polarization analyzers. In order to take into account the improvement in the measurements provided by redundancy data (obtained when increasing the number of polarization analyzers), the use of the *EWV* is recommended.

When incomplete polarimeters were analyzed, numeric simulations shown that the *EWV* gives the best global result, but not necessarily the minimum error propagation in all the Stokes parameters. Then, the minimization of the variance of a specific Stokes parameter can be helpful for the use of a polarimeter in applications where only the detection of a range of SOPs is needed.

An implementation of the optimization process was carried on a Stokes polarimeter based on two monopixel Parallel Aligned Liquid Crystal Displays (LCD) used as variable retarders. Due to experimental errors, the obtained polarization analyzers differed from the theoretical ones. The results have shown that small variations not change significantly the *CN* or the *EWV* of the optimized polarimeter. We have implemented several complete polarimeters and an incomplete polarimeter. All of them have been tested by measuring diverse incident SOPs and the obtained results were compared with the obtained with a commercial polarimeter.

Acknowledgments